# Why a hole is like a beam splitter: A general diffraction theory for multimode quantum states of light

Zhihao Xiao,[1,*] R. Nicholas Lanning,[1] Mi Zhang,[2] Irina Novikova,[2] Eugeniy E. Mikhailov,[2] and Jonathan P. Dowling[1]

[1]*Hearne Institute for Theoretical Physics and Department of Physics & Astronomy, Louisiana State University, Baton Rouge, Louisiana 70803, USA*

[2]*Department of Physics, College of William & Mary, Williamsburg, Virginia 23187, USA*

(Received 29 March 2017; published 14 August 2017)

Within the second-quantization framework, we develop a formalism for describing a spatially multimode optical field diffracted through a spatial mask and show that this process can be described as an effective interaction between various spatial modes. We demonstrate a method to calculate the quantum state in the diffracted optical field for any given quantum state in the incident field. We also give several additional examples of how the theory works, for various quantum input states, which may be easily tested in the laboratory, including two single-mode squeezed vacuums, single- and two-photon inputs, where we show that the diffraction process produces a two-mode squeezed vacuum, number-path entanglement, and a Hong-Ou-Mandel-like effect analogous to that of a beam splitter.

DOI: 10.1103/PhysRevA.96.023829

## I. INTRODUCTION

Gaussian spatial modes, in comparison with plane waves, offer a more accurate description of optical beams [1]. Although plane waves are mathematically simpler, they are less powerful in describing the diffraction and the spatial structure of optical fields. Classical diffraction properties of Gaussian beams are relatively well understood, and numerous works have been carried out, both theoretical and experimental [2–9]. The quantum properties of diffracted Gaussian beams, or other paraxial beams, have received less attention, although some previous works are reported in Refs. [10–26]. For example, complementary work by Lupo *et al.* [27] shows that diffraction through an iris can be described as a memory channel, which has applications to quantum communication, while our work focuses on classical and quantum behaviors of very specific Gaussian beams, with multiple spatial modes, for use in quantum imaging and related technologies. Though many previous analyses do take multiple Gaussian modes under consideration, a clear and systematic description of the interaction among Gaussian modes is lacking. By Gaussian-mode interaction we mean all physical processes in which the output spatial mode decomposition is altered from its input decomposition. The assumption, made in many cases, that Gaussian modes interact in the same way as plane waves, is generally not valid because it essentially ignores the multimode structure of Gaussian modes. Gaussian modes are a natural choice to describe the propagation of optical beams with finite cross sections. Indeed, if the squeezed states generated in different Gaussian modes have different squeezing angles, then the interaction among the states in the various modes can worsen rather than improving the overall squeezing. Recent work further confirms the deficiency of using plane waves to analyze quantum states of light and motivates us to investigate the quantum behavior of Gaussian beams [28–30].

To understand the quantum behavior of Gaussian beams, we must understand how quantum states in different Gaussian modes interact with each other. Perhaps the simplest interaction between Gaussian modes can be introduced by applying a spatial mask to the beam axis and seeing how this changes the quantum states. Through this relatively simple model, we can establish a method to analyze more complicated problems.

In Sec. II, we use classical electrodynamics to analyze the Gaussian beam and the interactions among different orders of Gaussian modes. In Sec. III, we present a quantum description of states in Gaussian beams and their interactions. In Sec. IV, we consider three examples of applying our formalism to describe the propagation of various quantum input optical fields through an iris mask. The first one uses two single-mode squeezed vacuums as input, which has been tested experimentally [28], and our predictions agree well with the experimental observations. The other examples study the cases of single-photon and two-photon inputs, in which case our calculations predict the generation of a photon-number entanglement and a Hong-Ou-Mandel (HOM)–like effect, implying that an opaque spatial mask displays characteristics of a regular but lossy optical beam splitter.

## II. CLASSICAL ELECTRODYNAMIC DESCRIPTION OF GAUSSIAN-BEAM SPATIAL MODES

For an optical beam, the electromagnetic field satisfies Maxwell's equations in the so-called paraxial approximation. Furthermore, it is known that the Hermite-Gaussian (HG) and Laguerre-Gaussian (LG) modes are solutions of the free-space wave equation in the paraxial approximation. In Cartesian coordinates the solutions are the HG modes, whereas in cylindrical coordinates the solutions are the LG modes. While we focus on the LG modes in this paper, similar arguments apply to the HG modes. The normalized field amplitude of LG modes can be expressed as

$$u_{l,p}(r,\phi,z) = \frac{C_{lp}^{\mathrm{LG}}}{w(z)}\left(\frac{r\sqrt{2}}{w(z)}\right)^{|l|}\exp\left(-\frac{r^2}{w^2(z)}\right)$$

*zxiao3@lsu.edu

 

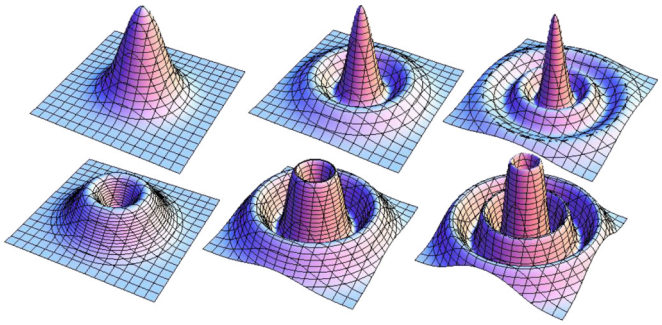

FIG. 1. Intensity profile of LG modes in any $z = z_0$ plane. Upper row (from left to right): $l = 0$, $p = 0,1,2$. Lower row: $l = 1$, $p = 0,1,2$.

$$\times L_p^{|l|}\left(\frac{2r^2}{w^2(z)}\right)\exp\left(-ik\frac{r^2}{2R(z)}\right)$$
$$\times \exp(il\phi)\exp\left[i(2p+|l|+1)\zeta(z)\right], \quad (1)$$

where $r$, $\phi$, and $z$ are cylindrical coordinates; $l$ and $p$ are the azimuthal and radial indices, which are integers; $p \geqslant 0$; $C_{lp}^{\mathrm{LG}} = \sqrt{\frac{2}{\pi}\frac{p!}{(|l|+p)!}}$ is a normalization constant; $L_p^{|l|}$ is the associated Laguerre polynomial; $k$ is the wave number; $w(z) = w_0\sqrt{1+(\frac{z}{z_R})^2}$ is the beam waist; $w_0$ is the beam waist at the beam focus; $z_R = \frac{\pi w_0^2}{\lambda}$ is the Rayleigh range; $R(z) = z[1+(\frac{z_R}{z})^2]$ is the radius of curvature; and $\zeta(z) = \arctan(\frac{z}{z_R})$ is the Gouy phase. See Fig. 1 for the intensity profile of several LG modes in any $z = z_0$ plane. Along the beam axis the profile becomes wider or narrower with changes in the beam waist, while the shapes of the profiles remain similar.

In free space the LG modes propagate independently without interacting with each other; they obey the following orthonormality conditions:

$$\int_{z=z_0} u_{l,p}u^*_{l',p'}rdrd\phi = \delta_{ll'}\delta_{pp'}. \quad (2)$$

Note: The orthogonality condition only holds if the integration area on the left-hand side of Eq. (2) is the entire $z = z_0$ plane.

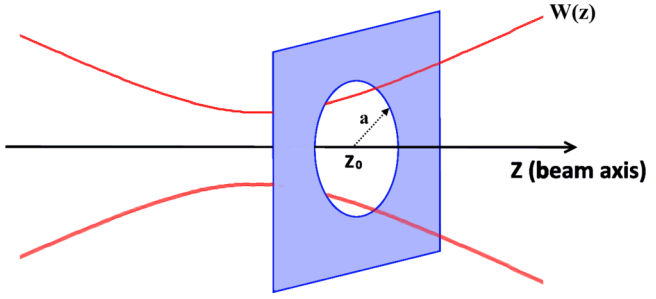


FIG. 2. The iris, with a circular opening of radius $a$, is applied along the beam axis. The red curve represents the Gaussian beam width $w(z)$ as a function of $z$. The iris is located on the plane $z = z_0$. The center of the iris is on the $z$ axis. The amplitude will be truncated to 0 at the rim of the iris, while in the opening of the iris the amplitude will be unchanged. As a result the orthogonality between LG modes will be broken, and the modes will interact in the iris plane.

Now, let us consider putting a spatial mask (such as a circular iris) in the $z = z_0$ plane, shown in Fig. 2. The iris blocks or absorbs the field at the rim and allows the field at the opening to pass through. For LG modes, the part of them allowed to pass through the opening of the iris no longer obeys orthogonality. Physically this means that different LG modes will interact at the plane where the iris is placed. The interaction of modes can be described by the expression

$$\int_S u_{l,p}u^*_{l',p'}rdrd\phi = B_{l,l',p,p'}, \quad (3)$$

where $S$ is the surface through which the spatial mask permits the light to pass. For a circular iris with radius $a$, centered on the beam axis, and placed in the $z = z_0$ plane, $S = \{r < a; z = z_0\}$.

Since in free space LG modes form an orthonormal basis, both the input signal (at $z = z_0^-$) and the output signal (at $z = z_0^+$) can be expressed as linear combinations of LG modes, which both satisfy paraxial approximation. Further, in free space on both sides of the iris $[z \in (-\infty, z_0) \cup (z_0, +\infty)]$, the orthogonality of LG modes holds, and the iris ($z = z_0$) is the only location where orthogonality is broken. Therefore the coefficient of each LG mode will change only when the signal goes through the iris. We express this interaction using the following set of equations: the input beam takes the form

$$u_{\mathrm{input}}(r,\phi,z) = \sum_{l,p} A_{l,p} \times u_{l,p}(r,\phi,z); \quad (z < z_0), \quad (4)$$

where $A_{l,p}$ is the coefficient of each LG mode. At the iris the beam is partially absorbed and thus we have

$$u_{\mathrm{iris}}(r,\phi,z_0) = \begin{cases} \sum_{l,p} A_{l,p} \times u_{l,p}(r,\phi,z_0) & (r < a, z = z_0), \\ 0 & (r \geqslant a, z = z_0), \end{cases} \quad (5)$$

satisfying the boundary condition at the iris, giving the output signal,

$$u_{\mathrm{iris}}(r,\phi,z_0) = u_{\mathrm{output}}(r,\phi,z_0^+), \quad (6)$$

which, finally, leads to

$$u_{\mathrm{output}}(r,\phi,z) = \sum_{l,p} A_{l,p} \sum_{l',p'} B_{l,l',p,p'}u_{l',p'}(r,\phi,z) \quad (z > z_0). \quad (7)$$

The quantity $B_{l,l',p,p'}$, first introduced in Eq. (3), is the transformation coefficient between LG mode $l, p$ and LG mode $l', p'$. Solving Eqs. (4)–(7), we get

$$B_{l,l',p,p'} = C_{l,l',p,p'} \times \exp[i(2p - 2p' + |l| - |l'|)\zeta(z_0)]. \quad (8)$$

Here we express the complex quantity $B_{l,l',p,p'}$ in polar form, as it more clearly shows the role of $\zeta(z_0)$, which is the Gouy phase at the iris position. The factor $C_{l,l',p,p'}$ is real in the circular iris situation, since the cylindrical symmetry prevents interaction between azimuthal indexes:

$$C_{l,l',p,p'} = \delta_{ll'} \times \int_0^{2a^2/w^2(z_0)} \exp(-x)L_p^{|l|}(x)L_{p'}^{|l'|}(x)dx. \quad (9)$$

It is because of the limitation in the radial direction, introduced by the iris, that different $p$ modes will interact. But

due to the cylindrical symmetry of the iris, different $l$ modes will remain orthogonal. Therefore, if, instead of a circular iris, other types of spatial masks (that do not have cylindrical symmetry) are used, orthogonality among $l$ modes will be broken, and different $l$ modes will interact with each other. The interactions, which are characterized by the transformation coefficient, will be determined by the shape and position of the spatial mask. For the remainder of this paper, we consider only an iris spatial mask because of its simplicity. However, our theory applies to all spatial masks, and the transformation coefficients can be calculated in a similar manner. To calculate transformation coefficients for an arbitrary spatial mask, we can still make use of the more general Eq. (3) instead of Eqs. (8) and (9), which are specifically suitable for a circular iris mask centered on the beam axis.

## III. QUANTIZATION OF GAUSSIAN MODES

In free space, due to orthogonality, each mode of the Gaussian beam propagates without interacting with another mode. Therefore, the quantum state of each mode will evolve independently. A pure quantum state without mode entanglement is a product state of every quantum state in every Gaussian mode:

$$|\psi\rangle = \prod_{l=-\infty,\, p=0}^{l=+\infty,\, p=+\infty} |\psi_{l,p}\rangle\,. \tag{10}$$

The separable state forms a building block for more complicated states. A general pure state, with or without mode entanglement, can be expressed as a linear combination of separable states in the form of Eq. (10). Further, a mixed state can be expressed as a probabilistic sum of pure states.

When a spatial mask such as an iris is applied to a Gaussian beam, the quantum states of different modes will interact. The interaction can be described as the transformation of annihilation or creation operators of input modes into operators of output modes. This transformation should be unitary, which preserves the commutation relations of the annihilation or creation operators. However, one problem needs to be solved. Generally, spatial masks (or other optical devices) are lossy. For example, an iris will absorb part of the input signal at the rim. A widely accepted procedure [31] to deal with loss in quantum optics is to introduce "absorption modes," which we denote $A_1, A_2, \ldots$. To be clear, we call the original Gaussian modes "signal modes," since they are the ones that may contain information, such as squeezing levels and squeezing angles. We denote the signal modes simply with $l$ and $p$ numbers. Further, a prime symbol on the operators of output modes differentiates them from the operators of the input modes. The transformation, caused by the iris, from the operators of input modes into those of output modes is illustrated in Fig. 3.

Before we continue, let us explain a bit more about the absorption modes. They serve three purposes. The first purpose is that they describe the absorption (loss) of the field. Since the states in output-signal modes are described by tracing the entire output density matrix over the absorption modes, the total energy of the signal is generally decreased. The second purpose is that they help to keep the transformation unitary by expanding the dimension of the transformation matrix [32].

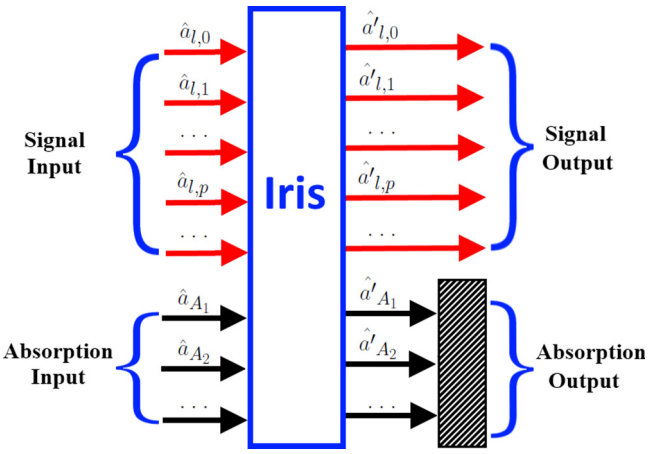


FIG. 3. The iris transforms the creation and annihilation operators of the input modes into operators of the output modes. Since the rim of the iris blocks off part of the beam, absorption modes (denoted $A_1$, $A_2$, etc.), in addition to the original Gaussian beam modes (signal modes), are needed. Input states in the absorption modes are vacuums. To obtain the reduced density operator in the output-signal modes, states in the output absorption modes need to be traced out.

The reader might remember that a similar principle applies when modeling loss with a simple beam splitter; we must consider a second input even if only the first input is used [31]. The third purpose of the absorption modes is that they naturally introduce the vacuum fluctuations and accommodate the common observation that fluctuations usually occur with losses.

The model works in the following way. The quantum states of the input-signal modes can be arbitrary, but quantum states in the input-absorption modes are vacuum. A unitary transformation transforms the operators of input-signal or absorption modes into operators of output-signal or absorption modes; this is illustrated in Fig. 3. Once we obtain output operators in terms of input operators we can calculate the quantum states in the output-signal or absorption modes. The quantum state in all output modes then needs to be traced over the output absorption modes, and finally, we obtain the reduced density matrix that describes the quantum state in the output-signal modes, which generally is a mixed state, even if the input state is a pure state. Later we give a few examples of a variety of input states.

### Matrix description of Gaussian mode interactions

The interaction among the quantum states of all LG modes can be described by a transformation from the operators of input modes (signal and absorption) to the operators of output modes. Such a transformation, as previously argued, is unitary for spatial masks. There are infinitely many Gaussian modes (and we need to introduce infinitely many absorption modes as well). Therefore, in the most general case, quantum states or operators in infinitely many input modes are transformed into quantum states or operators in infinitely many output modes.

Although this might seem complicated, sometimes the transformation can be greatly simplified when the spatial mask has some kind of symmetry. For example, as we previously pointed out, an iris has cylindrical symmetry and LG modes with different $l$'s do not interact [due to the Kronecker delta

in Eq. (9), which enforces angular momentum conservation]. Therefore, for a circular iris, we need only to examine the transformation of LG modes with the same $l$ but different $p$'s. To that end, we introduce the column vector of annihilation operators for input LG mode $(l, p = 0)$, $(l, p = 1)$, $(l, p = 2)$, etc., as well as operators for input-absorption modes $A_1$, $A_2$, $A_3$, etc.:

$$(\hat{a}_l) = \left(\hat{a}_{l,0}\ \hat{a}_{l,1}\ \ldots\ \hat{a}_{A_1}\ \hat{a}_{A_2}\ \ldots\right)^T. \tag{11}$$

The creation operators are, similarly,

$$(\hat{a}_l{}^\dagger) = \left(\hat{a}^\dagger_{l,0}\ \hat{a}^\dagger_{l,1}\ \ldots\ \hat{a}^\dagger_{A_1}\ \hat{a}^\dagger_{A_2}\ \ldots\right)^T, \tag{12}$$

and the output modes follow, but they are labeled with a prime:

$$(\hat{a}'_l) = \left(\hat{a}'_{l,0}\ \hat{a}'_{l,1}\ \ldots\ \hat{a}'_{A_1}\ \hat{a}'_{A_2}\ \ldots\right)^T, \tag{13}$$

$$(\hat{a}'^\dagger_l) = \left(\hat{a}'^\dagger_{l,0}\ \hat{a}'^\dagger_{l,1}\ \ldots\ \hat{a}'^\dagger_{A_1}\ \hat{a}'^\dagger_{A_2}\ \ldots\right)^T. \tag{14}$$

We also define the unitary transformation matrix $\mathcal{J}_l$, which determines the interaction among LG modes with the same $l$ but different values of $p$:

$$\mathcal{J}_l = \begin{bmatrix} J_{l;0,0} & J_{l;0,1} & \cdots & J_{l;0,A_1} & J_{l;0,A_2} & \cdots \\ J_{l;1,0} & J_{l;1,1} & \cdots & J_{l;1,A_1} & J_{l;1,A_2} & \cdots \\ \cdots & \cdots & \cdots & \cdots & \cdots & \cdots \\ J_{l;A_1,0} & J_{l;A_1,1} & \cdots & J_{l;A_1,A_1} & J_{l;A_1,A_2} & \cdots \\ J_{l;A_2,0} & J_{l;A_2,1} & \cdots & J_{l;A_2,A_1} & J_{l;A_2,A_2} & \cdots \\ \cdots & \cdots & \cdots & \cdots & \cdots & \cdots \end{bmatrix}. \tag{15}$$

The transformation of input and output operators can be expressed in the following compact form:

$$(\hat{a}_l{}') = \mathcal{J}_l(\hat{a}_l), \tag{16}$$

$$(\hat{a}'^\dagger_l) = \mathcal{J}^*_l(\hat{a}_l{}^\dagger). \tag{17}$$

$\mathcal{J}^*_l$ stands for the conjugate (without transpose) of $\mathcal{J}_l$. The signal-signal elements ($J_{l;0,0}$, $J_{l;1,0}$, $J_{l;0,1}$, etc.) in matrix $\mathcal{J}_l$ determine the transformation between input- and output-signal modes. Here we make use of Bohr's correspondence principle. For high-amplitude coherent states in the input-signal modes, the transformation between input- and output-signal modes should agree with the classical result in Eq. (7), giving

$$J_{l;p_1,p_2} = B_{l,l,p_1,p_2}, \tag{18}$$

which can be calculated using Eqs. (8) and (9). As for the other (signal-absorption and absorption-absorption) elements in $\mathcal{J}_l$, we can make use of $\mathcal{J}_l$'s being unitary. This gives $\mathcal{J}_l\mathcal{J}_l^\dagger = I$, which will give equations describing the relations among the $\mathcal{J}_l$ elements. Of course, signal-absorption and absorption-absorption elements might not be completely fixed, and there might be a certain freedom of choice. In fact, they may not need to be calculated at all. We find that, in the calculations we have done so far, we can always eliminate signal-absorption and absorption-absorption elements using the condition that $\mathcal{J}_l$ is unitary.

Indeed, if one aims for completeness, one should consider infinitely many LG modes. However, we do not usually have that luxury, since the dimension of the transformation matrix increases with the number of modes, and we are forced to consider a limited number of modes. Intuitively, the more modes we consider, the better. But the effect of higher-order modes often diminishes at a very fast rate. As we show in the next section, we are able to explain our experimental data, even if we consider only two input-signal modes and two absorption modes.

For a spatial mask of arbitrary shape, we cannot exploit the cylindrical symmetry as we did with the iris. However, we can still introduce a similar column vector of operators as before, but we now need to include various $l$ modes together instead of considering only one $l$ mode at a time. We can achieve this by defining a concatenation of column vectors of operators, such as $(\hat{a}) = [(\hat{a}_{l=0})^T\ \ (\hat{a}_{l=1})^T\ \ (\hat{a}_{l=-1})^T\ \ \ldots]^T$, in which every element is defined in Eq. (11). The transformation matrix $\mathcal{J}$ from input to output modes needs to be expanded in a similar fashion in order to accommodate different $l$ modes; and the integration area of Eq. (3) needs to be changed as well. Then we can, finally, arrive at a relation similar to Eq. (16): $(\hat{a}') = \mathcal{J}(\hat{a})$.

Unlike the iris, a spatial mask without cylindrical symmetry introduces interaction between orbital angular momentum modes, which can be very useful. However, the purpose of this work is not to explore novel designs of optical devices, but to set up a general method for analyzing a range of problems. For now, the simple iris is enough to serve such a purpose, but we stress that our method can also accommodate optical devices without cylindrical symmetry.

## IV. ADDITIONAL EXAMPLES OF THE USE OF THE THEORY

### A. Example 1: Squeezed-vacuum input states and the Wigner function description

Let us consider the following model. In the two signal LG modes of $(l = 0,\ p = 0)$ and $(l = 0,\ p = 1)$, we input

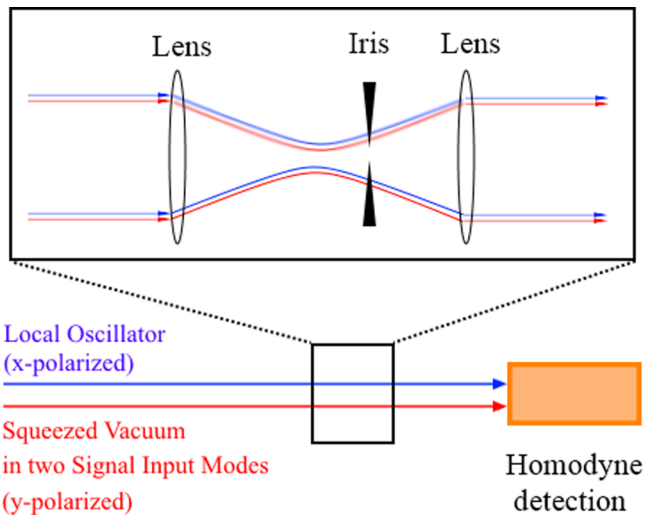


FIG. 4. Model setup. The single-mode squeezed vacuum states are in the $(l = 0,\ p = 0)$ and $(l = 0,\ p = 1)$ LG modes, while the local oscillator is in the $(l = 0,\ p = 0)$ LG mode. The squeezed vacuum and the local oscillator copropagate but are in perpendicular polarizations. The spatial mask consists of a one-to-one telescope and an iris between the lenses. We move the iris along the beam axis and find the minimum noise in each case.

two squeezed-vacuum quantum states, which are defined as $\hat{S}(\xi_0)\,|0\rangle_{l=0,\,p=0}$ and $\hat{S}(\xi_1)\,|0\rangle_{l=0,\,p=1}$, respectively, while in every other LG mode we input vaccum states. The squeezing operators are defined as $\hat{S}(\xi_p)=\exp[\frac{1}{2}(\xi_p^*\hat{a}_{0,p}^2-\xi_p\hat{a}_{0,p}^{\dagger 2})]$, with $p=0,1$. The squeezing parameters are $\xi_0=r_0\exp(i\theta_0)$ and $\xi_1=r_1\exp(i\theta_1)$.

Let us further consider a classical field with large amplitude, in the $(l=0,\ p=0)$ LG mode, acting as a local oscillator for homodyne detection. The signal and local oscillator copropagate with each other along the beam axis, but they are in perpendicular polarizations.

Now we insert a circular iris in the neighborhood of the beam focal point and centered on the beam axis, shown in Fig. 4. According to our theory, both the signal and the local oscillator are influenced by the iris in the way described in previous sections. Introduced by the iris, the interaction among LG modes mainly happens between the $(l=0,\ p=0)$ and the $(l=0,\ p=1)$ modes. Therefore we can simplify the calculation by considering only two input-signal (or output-signal) modes and two absorption modes, instead of taking into account infinitely many input (or output) modes. The diagram of this model is shown in Fig. 5. We then move the iris along the beam axis and numerically simulate the minimum noise measured in the homodyne detection vs the iris position, shown in Fig. 6. We can also use different-sized irises, which are represented by different curves. The experimental counterpart of this simulation is investigated in Ref. [28].

In order to gain a clearer and more intuitive view, we now examine our model in the Wigner representation. It is essential to understand how the iris transforms the input Wigner function into the output Wigner function. We first use Eqs. (16) and (17) to calculate the transformation between input and output mode operators and obtain the transformation of quadratures,

$$\begin{bmatrix} q_{l,0}\\ q_{l,1}\\ q_{A_1}\\ q_{A_2}\end{bmatrix}=\mathrm{Re}(\mathcal{J}_l)\begin{bmatrix} q'_{l,0}\\ q'_{l,1}\\ q'_{A_1}\\ q'_{A_2}\end{bmatrix}-\mathrm{Im}(\mathcal{J}_l)\begin{bmatrix} p'_{l,0}\\ p'_{l,1}\\ p'_{A_1}\\ p'_{A_2}\end{bmatrix}, \tag{19}$$

$$\begin{bmatrix} p_{l,0}\\ p_{l,1}\\ p_{A_1}\\ p_{A_2}\end{bmatrix}=\mathrm{Re}(\mathcal{J}_l)\begin{bmatrix} p'_{l,0}\\ p'_{l,1}\\ p'_{A_1}\\ p'_{A_2}\end{bmatrix}+\mathrm{Im}(\mathcal{J}_l)\begin{bmatrix} q'_{l,0}\\ q'_{l,1}\\ q'_{A_1}\\ q'_{A_2}\end{bmatrix}. \tag{20}$$

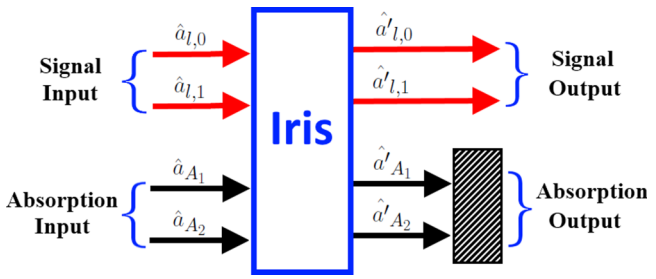


FIG. 5. Instead of taking into account infinitely many input or output modes, we consider only two input-signal (or output-signal) modes and two absorption modes, because the input states in the $(l=0,\ p=0)$ and $(l=0,\ p=1)$ LG modes are the only ones that are nonvacuum, and the interaction between the two modes far exceeds the interaction between other LG modes.

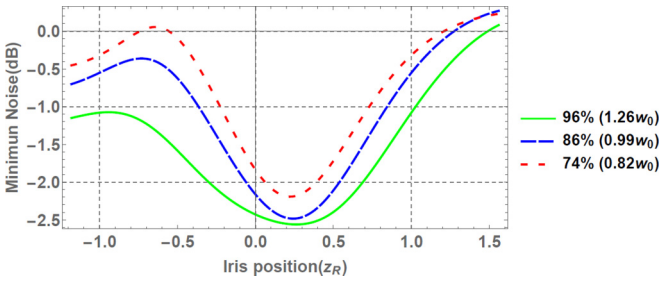


FIG. 6. Minimum noise in homodyne detection vs iris position. Different-sized irises are represented by different curves, and they are denoted by the percentage of peak transmission through the iris relative to full-beam transmission, as well as the iris radius (scaled by $w_0$). We apply only one iris at a time. The input states in the $(l=0,\ p=0)$ and $(l=0,\ p=1)$ LG modes are squeezed states with different squeezing parameters: $r_0=0.3, \theta_0=0, r_1=0.4$, $\theta_1=0.325\pi$.

Then we substitute the input quadratures with output quadratures, thus completing the transformation of the input Wigner function to the output Wigner function:

$$W(q_{0,0},p_{0,0},q_{0,1},p_{0,1},q_{A1},p_{A1},q_{A2},p_{A2}) \xrightarrow{\text{Eq.(19)(20)}} W(q'_{0,0},p'_{0,0},q'_{0,1},p'_{0,1},q'_{A1},p'_{A1},q'_{A2},p'_{A2}). \tag{21}$$

To make our example more general, we now replace the squeezed vacuum with displaced squeezed states as input states: $\hat{D}(\alpha_0)\hat{S}(\xi_0)\,|0\rangle_{l=0,\,p=0}$ and $\hat{D}(\alpha_1)\hat{S}(\xi_1)\,|0\rangle_{l=0,\,p=1}$ in the $(l=0,\ p=0)$ and $(l=0,\ p=1)$ LG modes. The displacement operator for the $l=0,\ p=1,2$ mode is defined as $\hat{D}(\alpha_p)=\exp(\alpha_p\hat{a}_{0,p}^{\dagger}-\alpha_p^*\hat{a}_{0,p})$. The Wigner functions of the quantum states in the two input-signal modes are

$$\begin{aligned} W(q_m,p_m)=\frac{1}{\pi}\exp\{&-e^{-2r_m}[(p_m-\bar{p}_m)\cos(\theta_m/2)\\ &-(q_m-\bar{q}_m)\sin(\theta_m/2)]^2\}\\ &\times\exp\{-e^{2r_m}[(q_m-\bar{q}_m)\cos(\theta_m/2)\\ &+(p_m-\bar{p}_m)\sin(\theta_m/2)]^2\}, \end{aligned} \tag{22}$$

where $q_m$ and $p_m$ are the quadratures of modes $(l=0,\ p=m)$ and $m=0,1$, and $\bar{q}_m=\frac{1}{\sqrt{2}}(\alpha_m+\alpha_m^*)$, $\bar{p}_m=\frac{i}{\sqrt{2}}(-\alpha_m+\alpha_m^*)$, $\xi_m=r_m\exp(i\theta_m)$. For absorption modes the input states are vacuums, whose Wigner functions are

$$W(q_n,p_n)=\frac{1}{\pi}\exp\big(-q_n^2-p_n^2\big), \tag{23}$$

where $n=A_1,A_2$. Since the total input state is the product state of states in each of the four input modes, the total input Wigner function is

$$\begin{aligned} &W(q_{0,0},p_{0,0},q_{0,1},p_{0,1},q_{A1},p_{A1},q_{A2},p_{A2})\\ &\quad=W(q_{0,0},p_{0,0})W(q_{0,1},p_{0,1})W(q_{A1},p_{A1})W(q_{A2},p_{A2}). \end{aligned} \tag{24}$$

We keep the input state fixed and change the position of the iris along the beam axis. The change in iris position changes the matrix elements of $\mathcal{J}_{l=0}$ in Eqs. (19) and (20), which in turn changes the output states in three ways: (a) the squeezing and antisqueezing level changes, (b) the squeezing angle changes,

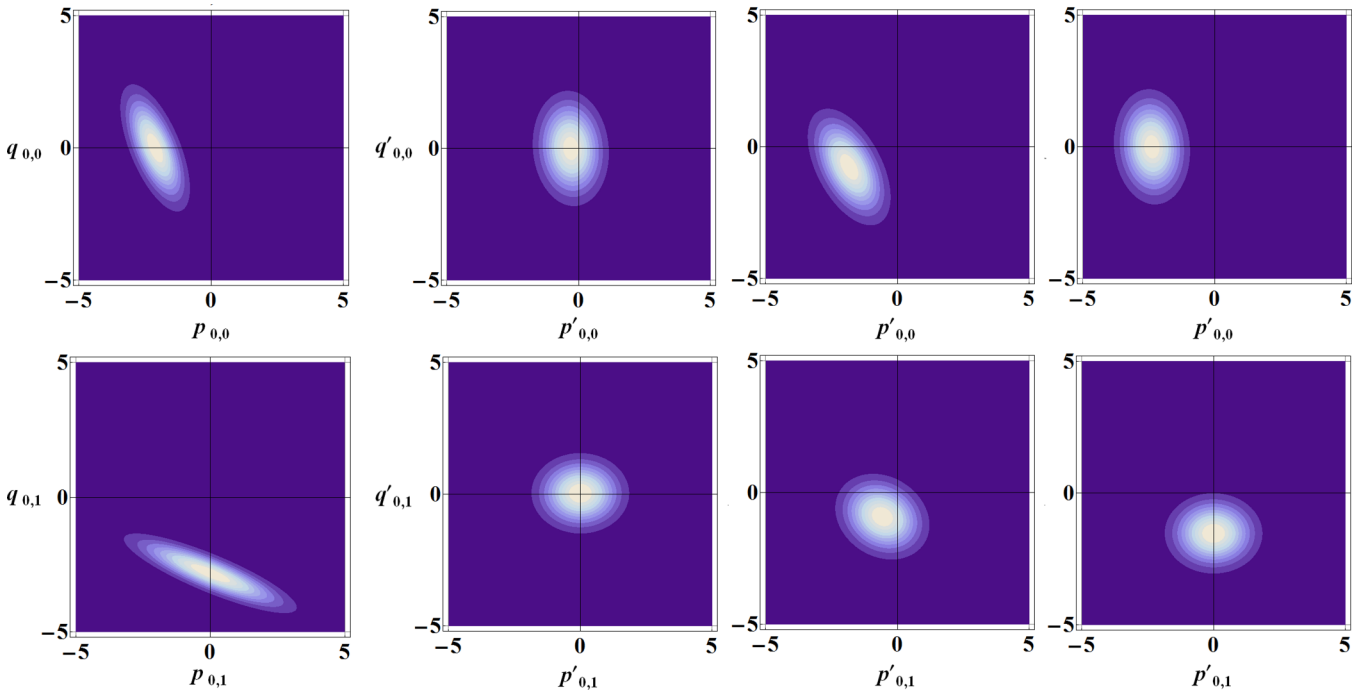


FIG. 7. First column on the left: Input displaced-squeezed-state Wigner function. Top row: LG mode $l = 0$, $p = 0$. Bottom row: LG mode $l = 0$, $p = 1$. The input states are displaced squeezed vacuums with displacement parameters $\alpha_0 = 1.5\exp(\pi i)$ and $\alpha_1 = 2\exp(1.5\pi i)$ and squeezing parameters $r_0 = 0.5$, $\theta_0 = 0.25\pi$, $r_1 = 0.8$, $\theta_1 = 0.75\pi$. Second column from left: Output quantum state Wigner function when the iris is located at $z = -z_R$ (one Rayleigh range before the focus). Third column: Output quantum state Wigner function when the iris is located at $z = 0$. Fourth column: Output quantum state Wigner function when the iris is located at $z = z_R$. The iris radius is $w_0$. This provides evidence that moving the iris rotates the squeezing angles via the Gouy phase. Note that the input-signal states shown here are pure states, while the output-signal states in both LG modes are mixed states.

and (c) the state displacement (from vacuum) changes. The Wigner functions of the input state (as well as the output states) of different iris positions are plotted in Fig. 7. It is also noteworthy that, despite the input-signal states in this example being pure states (displaced squeezed-vacuum states in each of the two LG modes), the output-signal states are generally mixed states. This is mainly because we obtain the reduced density operator for the signal modes by tracing the total density operator over the absorption modes. As a result, the output states are no longer pure minimum-uncertainty states. To verify this we can simulate the squeezing and antisqueezing noise in each output LG mode vs the iris position, shown in Fig. 8. For a minimum-uncertainty squeezed state, the squeezing and antisqueezing noise should add up to 0 dB, which means the squeezing and antisqueezing noise curve for the same mode should be symmetric about the horizontal axis in Fig. 8. This is obviously not the case, which verifies that the output-signal state is not a minimum-uncertainty state in either LG mode. The noise measurement in Fig. 8 is achievable in an experiment. For instance, we can make use of homodyne detection and adjust the local oscillator to be in one particular single-output LG mode with a spatial light modulator. Note that the noise measurement described in Fig. 6 is different. In that case, the local oscillator copropagates with the signal and both of them are influenced by the iris; after the iris the local oscillator consists of multiple LG modes instead of a single mode. We would like to emphasize that every example is applicable for any suitable detection scheme without being limited to homodyne detection. For example, in Sec. IV C below we predict a HOM-like effect for which coincident detection is required, and not homodyne.

Now we show a rather surprising result, namely, that the spatial mask behaves like a multiport beam splitter with loss. To elaborate this point, let us consider the following situation. In the case of the input states of a beam splitter being two

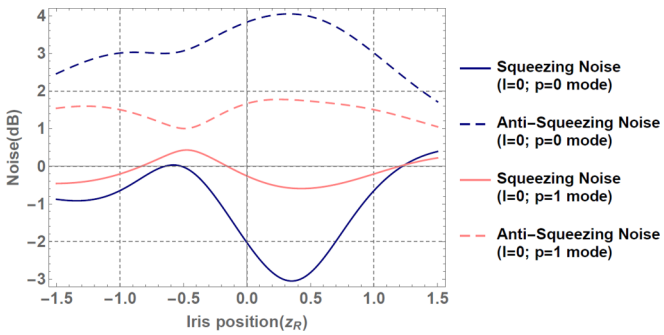


FIG. 8. Noise of squeezing and antisqueezing of the $l = 0$, $p = 0$ and $l = 0$, $p = 1$ LG modes vs iris position (in units of Rayleigh range). The parameters of the input states and iris size are the same as those for Fig. 7. Note that the squeezing and antisqueezing noise curve for the same mode are not symmetrical about the horizontal axis (0-dB noise -evel line) for displaced-squeezed input states. This is because the quantum state in each LG mode is no longer a minimum-uncertainty state.

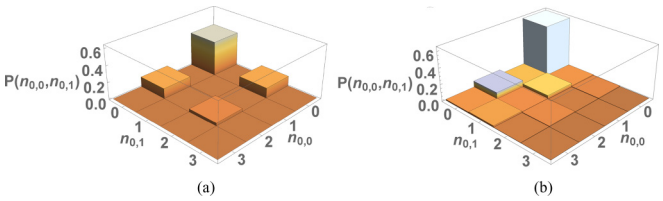


FIG. 9. Joint probability $P_{n_{0,0},n_{0,1}}$ vs $n_{0,0}$ vs $n_{0,1}$ in (a) the input LG ($l = 0$, $p = 0$) and ($l = 0$, $p = 1$) modes and (b) the same two LG modes in the output. Squeezing parameters of squeezed-vacuum states in the input modes are $r_0 = r_1 = 1$, $\theta_0 = \theta_1 = 0$. The iris is placed at $z = 0$ and the radius of the iris is $0.8339w_0$. Note that the nonzero probability for the one-one block provides evidence that the iris has converted the two separable squeezed-vacuum inputs into an entangled two-mode squeezed-vacuum output.

single-mode squeezed-vacuum states with identical squeezing parameters, it is well known [31] that the output state will be a two-mode squeezed state, if the beam splitter is perfectly 50:50. Now, let us use an iris instead of a beam splitter. We put identical single-mode squeezed-vacuum states in both input LG modes ($l = 0$, $p = 0$) and ($l = 0$, $p = 1$). After the states go through the iris, we then calculate the probability of detecting $n_{0,0}$ and $n_{0,1}$ photons in the output LG modes ($l = 0$, $p = 0$) and ($l = 0$, $p = 1$), shown in Fig. 9. For comparison, we show the probability in the input modes as well in Fig. 9. We can see in the input modes that, since the quantum state is a product state of two single-mode squeezed-vacuum, the probability is nonzero only at even $n_{0,0}$ and $n_{0,1}$. If the state in the output modes is indeed a two-mode squeezed state, the probability is nonzero only at $n_{0,0} = n_{0,1}$, namely, $n_{0,0} = n_{0,1} = 0$, $n_{0,0} = n_{0,1} = 1$, $n_{0,0} = n_{0,1} = 2$, etc. However, one important visible change from the two single-mode squeezed-vacuum states to a two-mode squeezed-vacuum state is that the two-mode joint probability $P_{n_{0,0}=1,n_{0,1}=1}$ is 0 in the former and nonzero in the latter [32]. This is indeed the case, as we can see in Fig. 9, which verifies our conjecture: a hole is like a beam splitter. We can also see that Fig. 9 does not give an ideal two-mode squeezed state; this is because the iris is unbalanced (the different modes have different radial profiles) and lossy, as opposed to a perfect 50:50 beam splitter.

We can see how $P_{n_{0,0}=1,n_{0,1}=1}$ and $P_{n_{0,0}=3,n_{0,1}=3}$ would change with the iris size in Figs. 10(a) and 10(b). Both of them reduce to 0 when the iris is completely closed, where the output state is reduced to a vacuum. Note that $P_{n_{0,0}=1,n_{0,1}=1}$ and $P_{n_{0,0}=3,n_{0,1}=3}$ also reduce to 0 in the case of large iris size, where the output state is reduced to the same as the input state (a product state of two single-mode squeezed-vacuum states). The nonzero $P_{n_{0,0}=1,n_{0,1}=1}$ and $P_{n_{0,0}=3,n_{0,1}=3}$ are what give the distinct feature of two-mode squeezing, which is most visible when the iris is neither too large nor too small, which is where the maximal interaction between LG mode ($l = 0$, $p = 0$) and LG mode ($l = 0$, $p = 1$) takes place.

We can also investigate the covariance of the photon numbers in the two input modes or the two output modes, which is defined as [32]

$$\mathrm{Cov}(n_{0,0},n_{0,1}) = \langle n_{0,0}n_{0,1}\rangle - \langle n_{0,0}\rangle \langle n_{0,1}\rangle . \qquad (25)$$

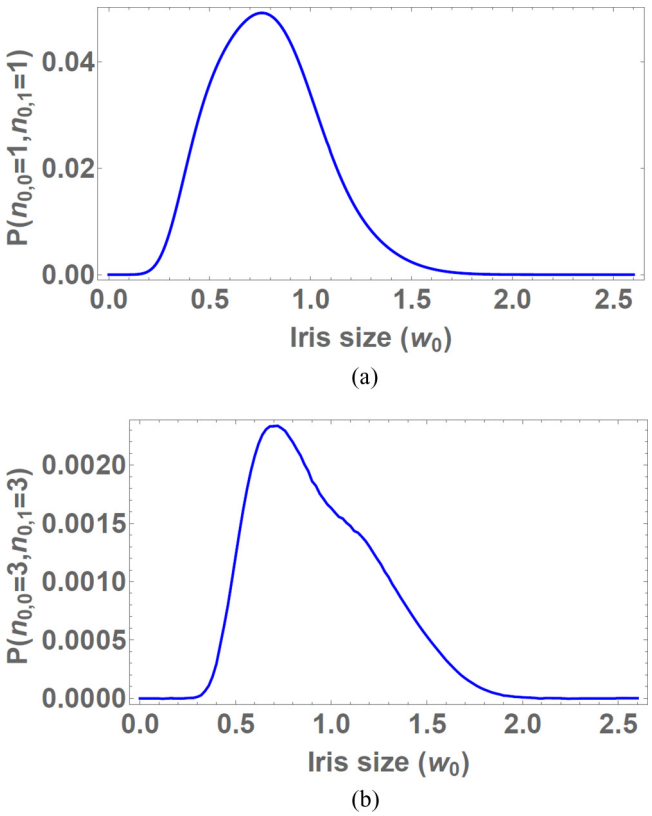


FIG. 10. (a) $P_{n_{0,0}=1,n_{0,1}=1}$ and (b) $P_{n_{0,0}=3,n_{0,1}=3}$ vs iris size (scaled by $w_0$) for the output states. Squeezing parameters of squeezed-vacuum states in the input modes are $r_0 = r_1 = 1$, $\theta_0 = \theta_1 = 0$. The iris is placed at $z = 0$. If the outputs were two separable, squeezed vacuums, then (a) the one-one probability and (b) the three-three probability would be identically 0, regardless of the iris radius. The fact that both these terms are nonzero supports the idea that the output is an entangled two-mode squeezed vacuum. In our beam-splitter analogy the effective beam splitter is closest to 50:50 when the iris size is about the beam waist in radius.

For single-mode squeezed-vacuum states in the two input modes, the covariance is obviously 0 since the state in each mode is independent. However, in the output modes of the iris, we should see generally nonzero covariance due to the beam-splitter-like interaction introduced by the iris, if indeed that interaction produces an entangled two-mode squeezed vacuum. In this case, where we consider only the LG ($l = 0$, $p = 0$) and ($l = 0$, $p = 1$) modes and two other absorption modes, the output covariance is

$$\begin{aligned}\mathrm{Cov}(n_{0,0},n_{0,1}) = {} & C^2_{0,0,0,0}C^2_{0,0,0,1}\sinh^2 r_0 \cosh^2 r_0 \\ & + C^2_{0,0,0,1}C^2_{0,0,1,1}\sinh^2 r_1 \cosh^2 r_1 \\ & + 2C_{0,0,0,0}C_{0,0,0,1}C^2_{0,0,0,1}\sinh r_0 \sinh r_1 \\ & \times (\sinh r_0 \sinh r_1 + \cosh r_0 \cosh r_1 \\ & \times \cos[4\zeta(z_0) + \theta_0 - \theta_1]), \end{aligned} \qquad (26)$$

where $z_0$ is the iris position and the $C_{l,l',p,p'}$'s can be calculated using Eq. (9). We can see in Eq. (26) the joint effect on the covariance of the Gouy phase $\zeta(z_0)$ and the squeezing angles $\theta_0$ and $\theta_1$ of the two input squeezed states. If $\theta_0$ and $\theta_1$ are

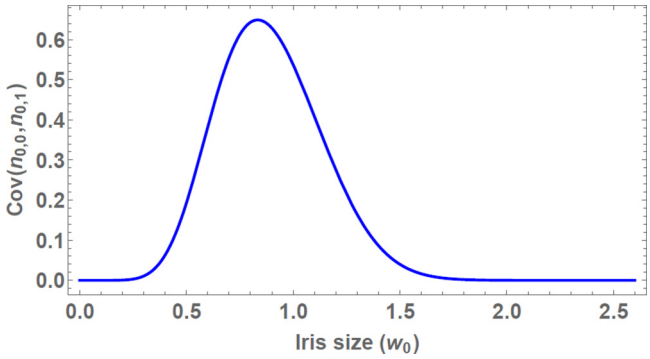


FIG. 11. Covariance of output LG modes vs iris radius. The squeezing parameters of the two separable, squeezed-vacuum states in the input modes are $r_0 = r_1 = 1, \theta_0 = \theta_1 = 0$. The iris is placed at $z = 0$. We can see that the covariance between the two output modes peaks at an iris radius of $0.8339w_0$, which is the radius we use in Fig. 9(b). Also, the reader might be interested to know that as long as the squeezing parameters in the LG ($l = 0$, $p = 0$) and ($l = 0$, $p = 1$) modes are the same, the covariance always peaks if the iris is placed at $z = 0$ and has a radius of $0.8339w_0$. In our beam-splitter analogy, if the outputs were again two separable, single-mode squeezed vacuums, the covariance would be identically 0 for all iris radii, which is clearly not the case. If the iris acted like a perfect 50:50 beam splitter, the covariance would be $\frac{1}{4}\sinh^2(2r) \approx 3.29$ [32]. However, due to loss and mode mismatch it peaks here at 0.65. Again, it peaks when the iris radius is about the beam waist, where the LG ($l = 0$, $p = 0$) and ($l = 0$, $p = 1$) mode overlap is maximal.

different to begin with, we can counteract this difference by altering the iris position $z_0$ to change the Gouy phase. We can see how the covariance would change with the iris radius in Fig. 11.

To sum up, when applied to a Gaussian beam, the spatial mask behaves very much like a multiport beam splitter with loss. If the input quantum states are displaced squeezed states, the spatial mask alters the displacement, which is a classical phenomenon; the spatial mask also alters the squeezing levels and angles, which is a nonclassical phenomenon. Note that even though the input squeezed states are pure, minimum-uncertainty states, the output states are generally mixed states with Wigner functions similar to displaced squeezed thermal states. The spatial mask also behaves similarly to a beam splitter, transforming the product state of two single-mode squeezed vacuums into, to an extent, an entangled two-mode squeezed state. Although this transformation is not perfect, since the spatial mask is lossy and unbalanced compared to a 50:50 beam splitter, there can be no doubt that even a device as simple as an iris should be treated quantum mechanically like a beam splitter.

### B. Example 2: A single photon in one input state and the generation of number-path entanglement

In this example we input a single-photon state in signal mode ($l = 0$, $p = 0$) and a vacuum state in signal mode ($l = 0$, $p = 1$) as well as absorption modes $A_1$ and $A_2$. (The input states for absorption modes are always vacuum.) Therefore the total input state in four modes is $|1\rangle_{l=0,\,p=0} \otimes |0\rangle_{l=0,\,p=1} \otimes |0\rangle_{A_1} \otimes |0\rangle_{A_2}$, shown in Fig. 12. For the vacuum state, the corresponding Wigner function is, again,

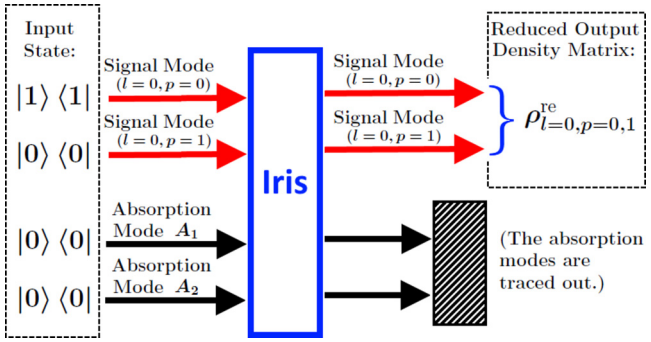


FIG. 12. As in the previous example, we consider two signal modes: LG modes ($l = 0$, $p = 0$) and ($l = 0$, $p = 1$), along with two absorption modes $A_1$ and $A_2$. The input state is a product state of a single photon in the ($l = 0$, $p = 0$) mode and a vacuum in other modes: $|1\rangle_{l=0,\,p=0} \otimes |0\rangle_{l=0}$, $p = 1 \otimes |0\rangle_{A_1} \otimes |0\rangle_{A_2}$. After the two output absorption modes are traced over, the reduced density matrix of the two output-signal modes, $\rho_{l=0}$ and $p = 0, 1^{re}$, is given in Eq. (36). We show in Fig. 13 that the output state shows number-path entanglement, created by the iris.

$$W_{N=0}(q,p) = \frac{1}{\pi}\exp[-(q^2+p^2)], \tag{27}$$

where $N$ is the photon number. For the single-photon state, the corresponding Wigner function is [31]

$$W_{N=1}(q,p) = \frac{-1}{\pi}\exp[-(q^2+p^2)]L_1(2q^2+2p^2), \tag{28}$$

where $L_N$ is the $N$th-order Laguerre polynomial. The overall Wigner function [for LG signal modes ($l = 0$, $p = 0$) and ($l = 0$, $p = 1$) and absorption modes $A_1$ and $A_2$] is, therefore,

$$\begin{aligned} &W(q_{0,0},p_{0,0},q_{0,1},p_{0,1},q_{A1},p_{A1},q_{A2},p_{A2}) \\ &\quad = W_{N=0}(q_{0,0},p_{0,0})W_{N=1}(q_{0,1},p_{0,1}) \\ &\qquad \times W_{N=0}(q_{A1},p_{A1})W_{N=0}(q_{A2},p_{A2}). \end{aligned} \tag{29}$$

Using the same method in the last example we calculate the Wigner function of the output modes. We then can calculate the Wigner function for either output mode, for example, the LG mode ($l = 0$, $p = 0$), by tracing over the other modes:

$$\begin{aligned} &W_{l=0,\,p=0}(q'_{0,0},p'_{0,0}) \\ &\quad = \int W(q'_{0,0},p'_{0,0},q'_{0,1},p'_{0,1},q'_{A1},p'_{A1},q'_{A2},p'_{A2}) \\ &\qquad \times dq'_{0,1}dp'_{0,1}dq'_{A1}dp'_{A1}dq'_{A2}dp'_{A2} \\ &\quad = (1-|J_{l=0;0,0}|^2)W_{N=0}(q'_{0,0},p'_{0,0}) \\ &\qquad + |J_{l=0;0,0}|^2 W_{N=1}(q'_{0,0},p'_{0,0}). \end{aligned} \tag{30}$$

Therefore, in the output-signal LG mode ($l = 0, p = 0$), the reduced density operator is

$$\rho^{re}_{l=0,\,p=0} = (1-|J_{l=0;0,0}|^2)\,|0\rangle\langle 0| + |J_{l=0;0,0}|^2\,|1\rangle\langle 1|\,. \tag{31}$$

With a similar calculation, we find that, in the output-signal LG mode ($l = 0,\ p = 1$), the reduced density operator is

$$\rho^{\rm re}_{l=0,\ p=1} = (1 - |J_{l=0;0,1}|^2)\,|0\rangle\,\langle 0| + |J_{l=0;0,1}|^2\,|1\rangle\,\langle 1|\,. \quad (32)$$

From Eqs. (31) and (32) we can immediately see that if we fire a single photon in the ($l = 0,\ p = 0$) mode and a vacuum in the ($l = 0,\ p = 1$) mode, the photon will have a $|J_{l=0;0,0}|^2$ chance of staying in the ($l = 0,\ p = 0$) mode at the output and a $|J_{l=0;0,1}|^2$ chance of switching to the ($l = 0,\ p = 1$) output mode. Similarly, it is not difficult to find that if we fire a single photon in the ($l = 0,\ p = 1$) mode and vacuum in the ($l = 0,\ p = 0$) mode, that photon will have a $|J_{l=0;1,1}|^2$ chance of staying in the ($l = 0,\ p = 1$) mode at the output and a $|J_{l=0;1,0}|^2| = J_{l=0;0,1}|^2$ chance of switching to the ($l = 0,\ p = 0$) output mode. We take another look at this result in Example 3.

However, only looking at each output mode separately does not give us the insight of correlation between modes. To achieve this we need to consider the reduced density operator for both the output-signal LG modes, ($l = 0,\ p = 0$) and ($l = 0,\ p = 1$); this state is generally mixed and, perhaps more interestingly, contains number-path entanglement, which again is also created when a single photon strikes an ordinary 50:50 beam splitter. To see this, let us examine the Wigner function in two output-signal modes:

$$\begin{aligned} &W_{l=0,\ p=0,1}(q'_{0,0}, p'_{0,0}, q'_{0,1}, p'_{0,1}) \\ &= \frac{1}{\pi^2}\exp\left[-\left(q'^2_{0,0} + q'^2_{0,0} + q'^2_{0,1} + q'^2_{0,1}\right)\right] \\ &\quad\times[(1 - |J_{l=0;0,0}|^2 - |J_{l=0;0,1}|^2) \\ &\quad + |J_{l=0;0,0}|^2 L_1\left(2q'^2_{0,0} + 2q'^2_{0,0}\right) \\ &\quad + |J_{l=0;0,1}|^2 L_1\left(2q'^2_{0,1} + 2q'^2_{0,1}\right) \\ &\quad + 2J_{l=0;0,0}J^*_{l=0;0,1}(p'_{0,0} - iq'_{0,0})(p'_{0,1} + ip'_{0,1}) \\ &\quad + 2J^*_{l=0;0,0}J_{l=0;0,1}(p'_{0,0} + iq'_{0,0})(p'_{0,1} - ip'_{0,1})]. \end{aligned} \quad (33)$$

The quantum state corresponding to the Wigner function given in Eq. (33) is a mixed state of (a) the vacuum state,

$$|\phi_1\rangle = |0\rangle_{l=0,\ p=0} \otimes |0\rangle_{l=0,\ p=1}\,, \quad (34)$$

with a probability of $1 - |J_{l=0;0,0}|^2 - |J_{l=0;0,1}|^2$, and (b) an entangled state of the form

$$\begin{aligned} |\phi_2\rangle = &\frac{J^*_{l=0;0,1}}{\sqrt{(|J_{l=0;0,0}|^2 + |J_{l=0;0,1}|^2)}}\,|0\rangle_{l=0,\ p=0} \otimes |1\rangle_{l=0,\ p=1} \\ &+ \frac{J^*_{l=0;0,0}}{\sqrt{(|J_{l=0;0,0}|^2 + |J_{l=0;0,1}|^2)}}\,|1\rangle_{l=0,\ p=0} \otimes |0\rangle_{l=0,\ p=1}\,, \end{aligned} \quad (35)$$

with a probability of $|J_{l=0;0,0}|^2 + |J_{l=0;0,1}|^2$. Therefore the reduced density matrix for the output-signal LG mode ($l = 0,\ p = 0$) and ($l = 0,\ p = 1$) is

$$\begin{aligned} \rho^{\rm re}_{l=0,\ p=0,1} = &(1 - |J_{l=0;0,0}|^2 - |J_{l=0;0,1}|^2)\,|\phi_1\rangle\,\langle\phi_1| \\ &+ (|J_{l=0;0,0}|^2 + |J_{l=0;0,1}|^2)\,|\phi_2\rangle\,\langle\phi_2|\,. \end{aligned} \quad (36)$$

One can verify this result by calculating the Wigner function of $\rho^{\rm re}_{l=0,\ p=0,1}$ and comparing it with Eq. (33). Other works have also been done to demonstrate the entanglement generation using spatial masks [33–35]. One can examine the violation of the Clauser-Horne (CH) Bell inequality [36,37] of the entangled state $|\phi_2\rangle$. The farther the Clauser-Horne combination drops below $-1$, the easier the violation can be observed [38]. Therefore by plotting the minimized Clauser-Horne combination vs the iris position, shown in Fig. 13, we can quantitatively determine the extent of the entanglement, which is generated by the iris, that can be observed.

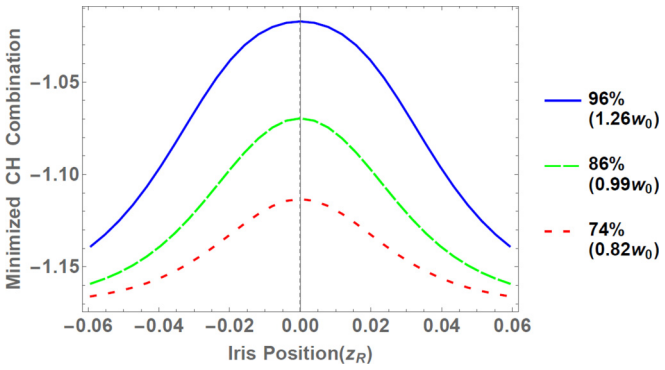


FIG. 13. Minimized Clauser-Horne (CH) combination vs iris position for different-sized irises. The CH combination is minimized in phase space. Note that the minimized CH combination is below $-1$, proving that the Bell inequality is violated. The farther the CH combination drops below $-1$, the more easily the violation can be observed. In our beam-splitter analogy it is well known [32] that a single photon incident on a 50:50 beam splitter produces the entangled state, $\frac{1}{\sqrt{2}}(|1\rangle\,|0\rangle + i\,|0\rangle\,|1\rangle)$.

### C. Example 3: A single photon in each of two input states and a Hong-Ou-Mandel-like effect

It is well known that when two identical photons are input into two separate modes of a beam splitter, photon bunching occurs. We show here that the iris produces a similar effect on two LG modes. Now let us input a single-photon state in mode ($l = 0,\ p = 0$) and another single-photon state in mode ($l = 0,\ p = 1$). Photon detectors are used to detect the photon numbers in the two output-signal LG ($l = 0,\ p = 0$) and ($l = 0,\ p = 1$) modes, then the photon detector count signals are fed into a correlator. The setup diagram is shown in Fig. 14. We then repeat this experiment multiple times so that we can measure the probability of detecting a single photon in each of the output-signal modes, which is refereed to as the coincidence probability. The goal is to produce a spatial mask version of the Hong-Ou-Mandel effect [39]. Previous works have already been done to demonstrate the HOM effect in multiple-spatial-mode experiments [40–42].

Let us first examine the case where, apart from being in different modes, the single-photon state in mode ($l = 0,\ p = 0$) and the single-photon state in mode ($l = 0,\ p = 1$) are completely distinguishable. This distinguishability can be caused by many things, such as the two photons having orthogonal polarizations or a large frequency difference or large time delay when they are fired. In this case when the two photons are completely distinguishable, they will not interfere and the case can be viewed simply as two

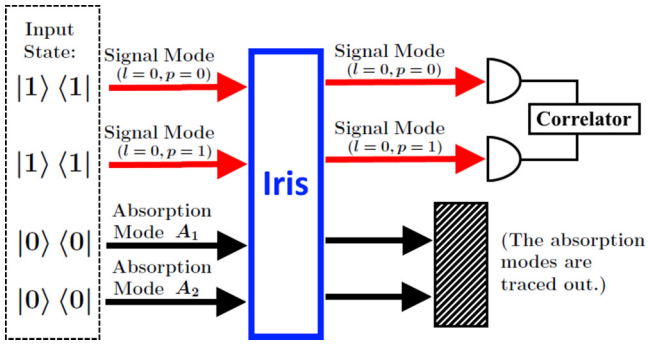


FIG. 14. Single-photon state in both of the two input-signal modes: the LG mode ($l=0,\ p=0$) and ($l=0,\ p=1$) and the vacuum state in the two input-absorption modes $A_1$ and $A_2$. Therefore the total input state of the four modes is $|1\rangle_{l=0},\ p=0 \otimes |1\rangle_{l=0},\ p=1 \otimes |0\rangle_{A_1} \otimes |0\rangle_{A_2}$. The coincidence probability of the two output-signal modes is given by the probability of the photon detectors receiving one photon each.

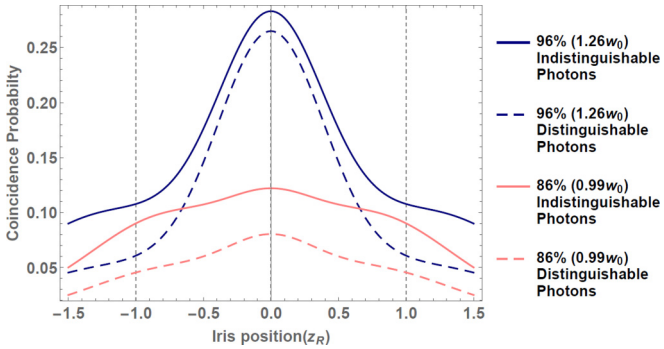


FIG. 15. Coincidence probability vs iris position. Lines of different colors represent different iris sizes, denoted by the percentage transmitted beam intensity through the iris at the focal point (relative to the full-beam intensity) as well as the iris radius (relative to $w_0$). Solid lines represent indistinguishable photons input in two signal modes; dashed lines, distinguishable photons. We can see that for irises of the same size and placed in the same position on the beam axis, inputting indistinguishable photons always leads to a higher coincidence probability than inputting distinguishable photons does. We call this a Hong-Ou-Mandel bump, and it is a hallmark of two-photon interference.

independent experiments combined: (a) input one photon in mode ($l=0,\ p=0$) and a vacuum in the other modes; (b) input one photon in mode ($l=0,\ p=1$) and a vacuum in the other modes. Therefore we can simply use the analysis in Example 2, and the coincidence probability is the probability that both photons will stay in the same modes at the output plus the probability that both photons will switch to the other modes, which is $J^2_{0;0,0} * J^2_{0;1,1} + |J_{0;1,0}|^2 * |J_{0;0,1}|^2 = J^2_{0;0,0} J^2_{0;1,1} + |J_{0;1,0}|^4$.

In the case where the two photons are completely indistinguishable, the coincidence probability can be calculated by the following procedure: (a) Similarly to Eq. (29), we find the total input-state Wigner function,

$$\begin{aligned} &W(q_{0,0}, p_{0,0}, q_{0,1}, p_{0,1}, q_{A1}, p_{A1}, q_{A2}, p_{A2}) \\ &\quad = W_{N=1}(q_{0,0}, p_{0,0}) W_{N=1}(q_{0,1}, p_{0,1}) \\ &\qquad \times W_{N=0}(q_{A1}, p_{A1}) W_{N=0}(q_{A2}, p_{A2}), \end{aligned} \tag{37}$$

(b) and we find the total output-state Wigner function $W(q'_{0,0}, p'_{0,0}, q'_{0,1}, p'_{0,1}, q'_{A1}, p'_{A1}, q'_{A2}, p'_{A2})$ using the transformation described in Eqs. (19) and (20); (c) and we find the reduced density matrix for the output-signal modes by tracing over the absorption modes,

$$\begin{aligned} &W_{l=0,\ p=0; l=0,\ p=1}(q'_{0,0}, p'_{0,0}, q'_{0,1}, p'_{0,1}) \\ &\quad = \int W(q'_{0,0}, p'_{0,0}, q'_{0,1}, p'_{0,1}, q'_{A1}, p'_{A1}, q'_{A2}, p'_{A2}) \\ &\qquad \times dq'_{A1} dp'_{A1} dq'_{A2} dp'_{A2}; \end{aligned} \tag{38}$$

(d) and we find the Wigner function for the state of a single photon in each output-signal mode, which is the state when coincidence is detected $\rho_{\text{coincidence}} = |1\rangle_{l=0,p=0}\langle 1| \otimes |1\rangle_{l=0,p=1}\langle 1|$,

$$\begin{aligned} &W_{\text{coincidence}}(q'_{0,0}, p'_{0,0}, q'_{0,1}, p'_{0,1}) \\ &\quad = W_{N=1}(q'_{0,0}, p'_{0,0}) \times W_{N=1}(q'_{0,1}, p'_{0,1}); \end{aligned} \tag{39}$$

(e) and we find the coincidence probability by projecting the output reduced density matrix onto the state $\rho_{\text{coincidence}}$ and calculating the trace,

$$\begin{aligned} &P_{\text{coincidence}} \\ &\quad = \text{tr}\left[\rho^{\text{re}}_{\text{l=0, p=0,1}} |1\rangle_{\text{l=0, p=0}}\langle 1| \otimes |1\rangle_{\text{l=0, p=1}}\langle 1|\right] \\ &\quad = \int W_{l=0,\ p=0; l=0,\ p=1} W_{\text{coincidence}} dq'_{0,0} dp'_{0,0} dq'_{0,1} dp'_{0,1} \\ &\quad = J^2_{0;0,0} J^2_{0;1,1} + |J_{0;1,0}|^4 + 2 J_{0;0,0} J_{0;1,1} |J_{0;1,0}|^2. \end{aligned} \tag{40}$$

Therefore, the coincidence probability for indistinguishable photons $J^2_{0;0,0} J^2_{0;1,1} + |J_{0;1,0}|^4 + 2 J_{0;0,0} J_{0;1,1} |J_{0;1,0}|^2$, is greater than the coincidence probability for distinguishable photons $J^2_{0;0,0} J^2_{0;1,1} + |J_{0;1,0}|^4$, since $J_{0;0,0}, J_{0;1,1}, |J_{0;1,0}|^2 \geqslant 0$, as shown in Fig. 15.

Therefore in the iris version of the HOM effect, when photons in the two input-signal modes are made to be indistinguishable, the coincidence probability rises. This is in contrast with the beam-splitter version of the HOM effect, in which the coincidence probability falls when photons in two input ports are made to be indistinguishable. In short, the iris produces a HOM "bump," while the beam splitter produces a HOM "dip."

The physical interpretation of the bump is that, while a beam splitter introduces a $\pi$ phase shift in the reflected beam, the spatial mask in our case does not produce any phase shift when the same two LG modes in the incident and diffracted beams are considered. This fermionlike antibunching behavior has been more thoroughly investigated in Ref. [43].

## V. CONCLUSION

We have analyzed Gaussian beams both classically and quantum mechanically. We have developed a clear method to calculate the interaction between quantum states in various Gaussian modes. While we focus on the mode interactions introduced by an iris, it is straightforward to extend our method

to other spatial masks or other optical devices. The framework we established allows us to analyze arbitrarily many Gaussian modes including various orbital angular momentum LG modes as well as HG modes. We verified our theory via our experiment, in which we generated squeezed states in various LG modes and found that the experimental data agreed with our numerical simulation. We, finally, gave three examples to show some interesting phenomena that can be easily tested in future experiments. These examples are displaced (and nondisplaced) squeezed-vacuum input states, along with single- and double-photon input states. These examples predict that the diffraction process gives rise to photon-number entanglement and a Hong-Ou-Mandel-like effect, which implies that the spatial mask behaves similarly to an ordinary beam splitter. As we pointed out, the purpose of this work is to set up a general method for analyzing quantum-state interaction between Gaussian modes, which can be useful in many ways, including creating a specific quantum state in higher-order modes from lower-order modes, creating entanglement between modes, optimizing overall squeezing, and designing specific interaction between different OAM modes.

## ACKNOWLEDGMENTS

This research was supported by Air Force Office of Scientific Research Grant No. FA9550-13-1-0098. In addition, Z.X., R.N.L., and J.P.D. would like to acknowledge support from the Army Research Office Grant No. W911NF-13-1-0381, the National Science Foundation Grant No. PHY-1403105, the Northrop Grumman Corporation and the Defense Advanced Research Projects Agency (US) Grant No. W911NF-17-1-0258.

[1] A. Siegman, *Lasers* (University Science Books, Sausalito, CA, 1986), p. 647.
[2] S. Zhang and T. Tamir, J. Opt. Soc. Am. A **6**, 1368 (1989).
[3] J. M. Liu, Opt. Lett. **7**, 196 (1982).
[4] P. Belland and J. P. Crenn, Appl. Opt. **21**, 522 (1982).
[5] J. E. Pearson, T. C. McGill, S. Kurtin, and A. Yariv, J. Opt. Soc. A. **59**, 1440 (1969).
[6] K. Uehara and H. Kikuchi, Appl. Phys. B **48**, 125 (1989).
[7] M. A. Porras, Phys. Rev. E **58**, 1086 (1998).
[8] S. S. R. Oemrawsingh, J. A. W. Van Houwelingen, E. R. Eliel, J. P. Woerdman, E. J. K. Verstegen, J. G. Kloosterboer, and G. W. 't Hooft, Appl. Opt. **43**, 688 (2004).
[9] N. Passilly, F. Treussart, R. Hierle, R. de Saint Denis, K. Aït-Ameur, and J.-F. Roch, J. Opt. Soc. Am. A **22**, 984 (2005).
[10] V. Peřinová and A. Lukš, J. Mod. Opt. **53**, 659 (2006).
[11] N. Treps, U. Andersen, B. Buchler, P. K. Lam, A. Maitre, H.-A. Bachor, and C. Fabre, Phys. Rev. Lett. **88**, 203601 (2002).
[12] N. Treps, N. Grosse, W. P. Bowen, C. Fabre, H.-A. Bachor, and P. K. Lam, Science **301**, 940 (2003).
[13] M. Lassen, G. Leuchs, and U. L. Andersen, Phys. Rev. Lett. **102**, 163602 (2009).
[14] K. Banaszek, A. B. Uren, and I. A. Walmsley, Opt. Lett. **26**, 1367 (2001).
[15] N. Corzo, A. M. Marino, K. M. Jones, and P. D. Lett, Opt. Express **19**, 21358 (2011).
[16] J. Janousek, K. Wagner, J.-F. Morizur, N. Treps, P. K. Lam, C. C. Harb, and H.-A. Bachor, Nat. Photon. **3**, 399 (2009).
[17] M. Beck, Phys. Rev. Lett. **84**, 5748 (2000).
[18] A. La Porta and R. E. Slusher, Phys. Rev. A **44**, 2013 (1991).
[19] C. Kim and P. Kumar, Phys. Rev. Lett. **73**, 1605 (1994).
[20] B. Chalopin, F. Scazza, C. Fabre, and N. Treps, Opt. Express **19**, 4405 (2011).
[21] L. Lopez, B. Chalopin, A. R. de la Souchère, C. Fabre, A. Maître, and N. Treps, Phys. Rev. A **80**, 043816 (2009).
[22] B. Chalopin, F. Scazza, C. Fabre, and N. Treps, in *European Quantum Electronics Conference* (Optical Society of America, Washington, DC, 2011), p. EA1_1.
[23] M. I. Kolobov, Rev. Mod. Phys. **71**, 1539 (1999).
[24] M. I. Kolobov, C. Fabre, P. Scotto, P. Colet, and M. San Miguel, in *Coherence and Quantum Optics VIII* (Springer, Berlin, 2003), pp. 173–184.
[25] B. Chalopin, F. Scazza, C. Fabre, and N. Treps, Phys. Rev. A **81**, 061804 (2010).
[26] A. Vaziri, G. Weihs, and A. Zeilinger, J. Opt. B: Quant. Semiclass. Opt. **4**, S47 (2002).
[27] C. Lupo, V. Giovannetti, S. Pirandola, S. Mancini, and S. Lloyd, Phys. Rev. A **85**, 062314 (2012).
[28] M. Zhang, R. N. Lanning, Z. Xiao, J. P. Dowling, I. Novikova, and E. E. Mikhailov, Phys. Rev. A **93**, 013853 (2016).
[29] M. Zhang, J. Soultanis, I. Novikova, and E. E. Mikhailov, Opt. Lett. **38**, 4833 (2013).
[30] T. Horrom, R. Singh, J. P. Dowling, and E. E. Mikhailov, Phys. Rev. A **86**, 023803 (2012).
[31] U. Leonhardt, *Measuring the Quantum State of Light*, *Vol. 22* (Cambridge University Press, Cambridge, UK, 1997), pp. 31, 62, 74.
[32] C. Gerry and P. Knight, *Introductory Quantum Optics* (Cambridge University Press, Cambridge, UK, 2005), pp. 138, 162, 185, 184, 194.
[33] X. Q. Yu, P. Xu, Z. D. Xie, J. F. Wang, H. Y. Leng, J. S. Zhao, S. N. Zhu, and N. B. Ming, Phys. Rev. Lett. **101**, 233601 (2008).
[34] M. Barbieri, F. De Martini, G. Di Nepi, and P. Mataloni, Phys. Rev. Lett. **92**, 177901 (2004).
[35] J. P. Torres, A. Alexandrescu, S. Carrasco, and L. Torner, Opt. Lett. **29**, 376 (2004).
[36] J. F. Clauser and M. A. Horne, Phys. Rev. D **10**, 526 (1974).
[37] M. Genovese, Phys. Rep. **413**, 319 (2005).
[38] C. F. Wildfeuer, A. P. Lund, and J. P. Dowling, Phys. Rev. A **76**, 052101 (2007).
[39] C. K. Hong, Z. Y. Ou, and L. Mandel, Phys. Rev. Lett. **59**, 2044 (1987).
[40] E. Karimi, D. Giovannini, E. Bolduc, N. Bent, F. M. Miatto, M. J. Padgett, and R. W. Boyd, Phys. Rev. A **89**, 013829 (2014).
[41] S. P. Walborn, A. N. de Oliveira, S. Pádua, and C. H. Monken, Phys. Rev. Lett. **90**, 143601 (2003).
[42] S. P. Walborn, W. A. T. Nogueira, A. N. de Oliveira, S. Pádua, and C. H. Monken, Mod. Phys. Lett. B **19**, 1 (2005).
[43] J. C. F. Matthews, K. Poulios, J. D. A. Meinecke, A. Politi, A. Peruzzo, N. Ismail, K. Wörhoff, M. G. Thompson, and J. L. O'Brien, Sci. Rep. **3**, 1539 (2013).